



Green approach and ease synthesis of C/N-codoped TiO₂ nanocrystals for photodegradation of endocrine

L. A. Al-Hajji · Adel. A. Ismail · M. Alseidi ·
F. Almutawa · S. Ahmad · A. Bumajdad

Received: 11 November 2019 / Accepted: 30 January 2020 / Published online: 14 February 2020
© Springer Nature B.V. 2020

Abstract Carbon species and nitrogen-codoped anatase TiO₂ (C/N-codoped TiO₂) nanocrystals with uniform particle size and high crystallinity were synthesized, employing hexamethylenetetramine (HMTA) as a nitrogen and carbon source throughout solvothermal reaction of TiCl₄ and HMTA at different contents (0.5 g, 1 g, 1.5 g, and 2 g HMTA). The synthesized photocatalysts were assessed by photocatalytic degradation of resorcinol as a probe of potent endocrine-disrupting chemicals (EDCs) compared with commercial P-25 photocatalyst. Raman spectra and XRD results confirmed that the obtained C/N-codoped TiO₂ is anatase TiO₂ phase with 10–20 nm nanocrystallite sizes. For resorcinol photo-oxidation in aerated aqueous solution, C/N-codoped TiO₂ nanocrystals synthesized at 0.5 g HMTA (H0.5) showed the superior photocatalytic efficiency among all synthesized photocatalysts. H0.5 photocatalyst exhibited the outstanding photocatalytic performance, which is 1.2 and 2 times greater than that

of commercial P-25 and pure TiO₂. In addition, the rate constant of the H0.5 sample was enhanced 7.5 and 3 times than that of commercial P-25 and pure TiO₂, respectively. The C/N-codoped TiO₂ nanocrystals achieved high photocatalytic efficiency of up to 96% within 90 min. In contrast, the photocatalytic efficiency based on the commercial P-25 was 54%. The photocatalytic efficiency of C/N-codoped TiO₂ was considerably enhanced, owing to its increase of photogenerated charge separation rate, smaller crystal size, narrower bandgap energy, and stronger light harvesting in wide visible region. Detailed mechanistic and kinetic studies through photodegradation of resorcinol in water were addressed.

Keywords Non-metal doped · TiO₂ nanoparticles · Nanostructured photocatalyst · Photodegradation · Endocrine · UV illumination

This article is part of the topical collection *Nanotechnology in Arab Countries*

Guest Editor: Sherif El-Eskandarany

L. A. Al-Hajji · A. A. Ismail (✉) · M. Alseidi ·
F. Almutawa · S. Ahmad
Nanotechnology and Advanced Materials Program, Energy &
Building Research Center, Kuwait Institute for Scientific Research
(KISR), P.O. Box 24885, 13109 Safat, Kuwait
e-mail: aaismail@kISR.edu.kw

A. Bumajdad
Department of Chemistry, Faculty of Science, Kuwait University,
P.O. Box 5969, 13060 Safat, Kuwait

Introduction

In the last three decades, comprehensive studies have been addressed for modifying TiO₂ nanoparticles to effectively harvest visible light and the natural sunlight for potential and photocatalysis application. In particular, doping of non-metals such as S, N, C, and F has considered the most efficient processes to drive UV and visible light photocatalysts (Fujishima and Zhang 2006). To promote the driven active photocatalyst under visible light illumination, non-metals codoped and

tridoped into TiO₂ have been synthesized such as carbon/nitrogen (Khedr et al. 2019; El-Sheikh et al. 2017), sulfur/nitrogen (El-Sheikh et al. 2014; Naik et al. 2010), and boron/fluoride (Liu et al. 2008). As compared to urea as carbon and nitrogen sources, carbon/nitrogen-codoped TiO₂ employing hexamethylenetetramine (HMTA) as the doping source showed better photocatalytic efficiency for photo-oxidation of bisphenol A (BPA) under visible light illumination. HMTA possesses high nitrogen content with a heterocyclic organic compound (Yin et al. 2003; Candelaria et al. 2012; Dreyfors et al. 1989). Whenever HMTA hydrolyzes in aqueous solution, it produces ammonia solution and the provided ammonia solution has been employed as the nitrogen source and precipitation agent to fabricate N-doped TiO₂ (Liu et al. 2009; Yin et al. 2005). The pH value of reaction solution could be influenced by adding HMTA, which may modify the TiO₂ crystalline phase-based photocatalyst; in addition, the nitrogen content doped in the final N-doped TiO₂ (Liu et al. 2009; Yin et al. 2005; Cheng et al. 2008). It was documented that the dopant content and crystal structure are two crucial factors that outstandingly influence its driven visible light photocatalyst. N/TiO₂ was employed for complete oxidation of BPA to CO₂ under UV illumination (Ohko et al. 2001; Atitar et al. 2015, 2019). As a result, it is substantial to investigate the impact of HMTA at different contents throughout the development of carbon and nitrogen-codoped TiO₂, employing the solvothermal approach. Phenolic compounds are widely applied and recognized in several manufacture effluents such as petrochemical units, paper, oil refineries, textile, pharmaceutical, steel industries, and synthetic rubber (Bilgili 2006; Dąbrowski et al. 2005). They were deemed as contaminants of essential intimidation to the environment due to higher oxygen demand, high toxicity, and low biodegradability (Ku and Lee 2000; Ahmad et al. 2019). Phenolic compounds were classified as the mean of the elementary contaminants by the United States Environmental Protection Agency (USEPA). Very low concentration of phenolic compounds could potentially possess severe effects on the living system because they are recognized as carcinogenic (Kumar et al. 2003). The maximum concentration of phenolic compounds is 1 ppm (mg kg⁻¹) in wastewater (Busca et al. 2008), and ingestion of trace phenol may cause vomiting, smoky or greenish colored urine, nausea, coma, and paralysis and may even cause death from cardiac arrest or

respiratory failure (Mohanty et al. 2005). Therefore, the removal of phenolic compounds is indispensable from industrial wastewater before throwing them to the natural influx. There are different techniques over the past few decades, employing to remove the phenolic compounds such as chemical oxidation, coagulation and precipitation, biodegradation, solid–liquid separation technique or adsorption, ion exchange, and photocatalytic degradation (Al-Hajji et al. 2020; Khedr et al. 2019; El-Sheikh et al. 2017, 2014; Naik et al. 2010).

In this contribution, C/N-codoped TiO₂ nanocrystals with uniform particle size and high crystallinity were synthesized, employing HMTA a nitrogen and carbon source throughout the solvothermal reaction of titanium tetrachloride (TiCl₄) and HMTA at different contents (0.5 g, 1 g, 1.5 g, and 2 g HMTA). The C/N-codoped TiO₂ nanocrystals achieved high photocatalytic efficiency of up to 96% within 90 min. In contrast, the photocatalytic efficiency based on commercial P-25 was 54%. At 0.5 g HMTA addition, the H0.5 photocatalyst exhibited the outstanding photocatalytic performance, which was 1.2 and 2 times greater than that of commercial P-25 and pure TiO₂. In addition, the rate constant of the H0.5 sample was enhanced 7.5 and 3 times than that of commercial P-25 and pure TiO₂, respectively.

Experimental

Materials

TiCl₄, HMTA, ethanol C₂H₅OH, and resorcinol were purchased from Sigma-Aldrich, Ltd.

Synthesis of TiO₂ nanoparticles

TiCl₄ (7.5 mL) was added dropwise into anhydrous ethanol (120 mL) throughout magnetic stirring for 30 min in an ice water bath to yield a yellowish solution as early published (Xu and Zhang 2010). Afterwards, HMTA was added at various contents (0.5 g, 1 g, and 2 g) to fabricate C/N-codoped TiO₂ nanocrystals, which were denoted as H0.5, H1, and H2, respectively. The obtained solution was put in 150 mL Teflon-lined immersed into the autoclave. The autoclave involving the mixture was maintained for 24 h at 150 °C and then cooled in the air to reach the room temperature. The obtained solid was separated by centrifugation and washed three times with ethanol and water. The

obtained wet powder was finally dried at 60 °C for 6 h and calcinated at 400 °C for 3 h to collect pure TiO₂, H0.5, H1, and H2 samples.

Characterization

The physicochemical properties of the synthesized samples were evaluated using the listed instruments as follows: Bruker D8 Advance powder X-ray diffractometer with Cu-K α ($\lambda = 0.15406$ nm) was employed to measure X-ray diffraction (XRD) patterns of the prepared C/N-codoped TiO₂ nanocrystals. The experimental XRD patterns are fitted using FullProf software based on the Rietveld refinement method (Rodriguez-Carvajal 1993). Raman spectroscopy of surface phases of C/N-codoped TiO₂ nanocrystals was employed to investigate the Raman spectra using a Renishaw inVia Raman microscope. JEOL JEM 1230 microscope was employed operating at 120 kV to determine high-resolution transmission electron microscopy (HRTEM) images. UV-vis spectrophotometer (UV-2600, Shimadzu) was used to determine UV-vis diffuse reflectance spectra (DRS) from 200 to 800 nm for all synthesized C/N-codoped TiO₂ nanocrystals, and BaSO₄ was employed as a reflectance standard. The bandgap value (E_g) was measured via the Tauc equation. The N₂ adsorption–desorption isotherms of the synthesized photocatalysts were measured by a computer-controlled sorption analyzer equipped with an outgassing platform (SAP 2010 automatic Micromeritics sorption analyzer (USA)). RF-6000 spectrofluorophotometer was employed (Japan, Shimadzu, 400 W, 50/60 Hz) to determine photoluminescence (PL) for the synthesized C/N-codoped TiO₂ nanocrystals using xenon lamp excitation source (150 W) at ~ 250 nm.

Photocatalytic tests

The photocatalytic degradation resorcinol (20 ppm) as a model molecule for endocrine disrupter in water over the prepared C/N-codoped TiO₂ nanocrystal photocatalysts was carried out. Either UV or UV-vis lamps (500 W Xe arc lamp) were vertically overwhelmed into the reactor. The 500 mL resorcinol solution (20 ppm) was mixed 0.5 g of C/N-codoped TiO₂ photocatalyst and was aerated, employing a pump to provide oxygen throughout photocatalytic reactions. The mixture was stirred in the dark for 30 min, applying a magnetic bar to obtain equilibrium of adsorption/

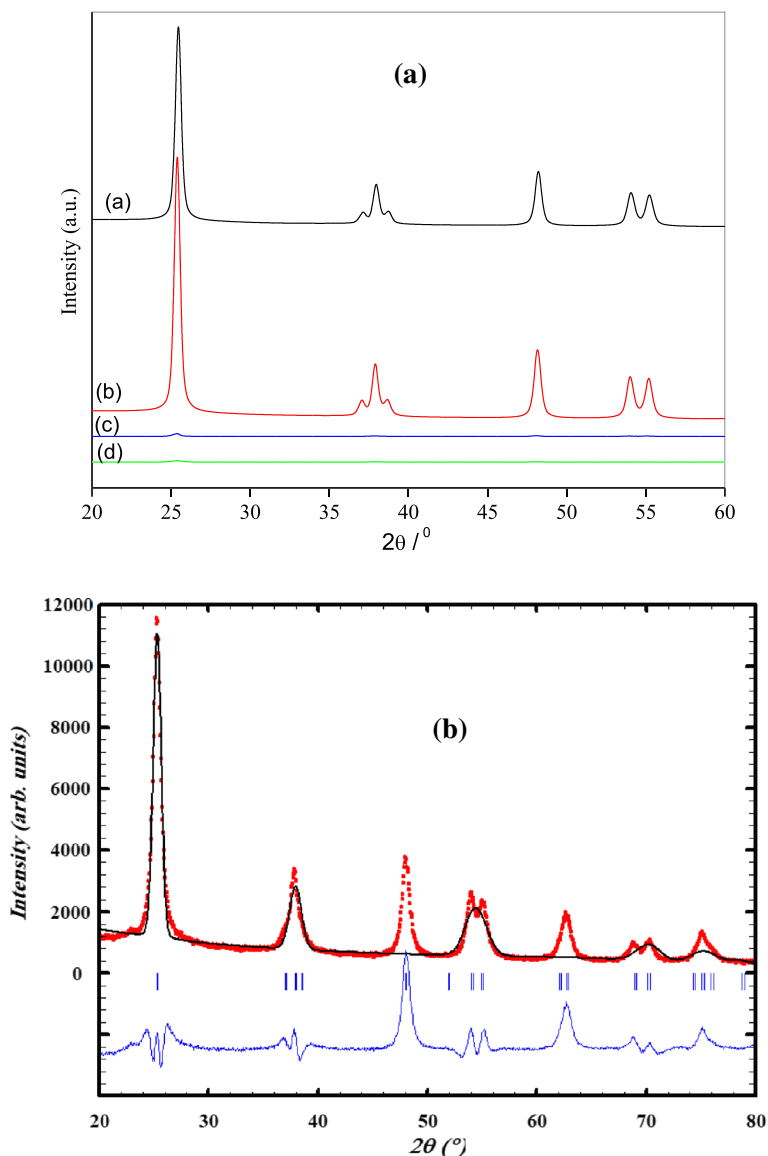
desorption of resorcinol before illumination. Then, the 500 W Xe arc lamp was switched on for 3-h illumination. During the photoreaction experiments, 3 mL of suspension solution was withdrawn at different reaction times systematically. The solid was separated from the filtrate using a centrifuge. Total organic carbon throughout the photocatalytic experiments was measured by the resorcinol mineralization (multi N/C 3100; Analytik Jena AG, Germany).

Results and discussions

Photocatalyst investigations

HMTA was employed as the source of the nitrogen and carbon dopants through the synthesis of C/N-codoped TiO₂ photocatalyst throughout the solvothermal reaction of TiCl₄ and HMTA at different contents (0 g, 0.5 g, 1 g, and 2 g). Figure 1 A displays the XRD patterns of the solvothermal-synthesized pure TiO₂, H0.5, H1, and H2 photocatalysts. The XRD peaks are sharp and narrow for pure TiO₂ and H0.5 samples, indicating the formation of crystalline material. The relative peak intensities presented are matching with those filed in JCPDS 21-1272 for anatase. The peaks indicated it corresponds to the following at 2θ with hkl indices: 25.40° (101), 37.96° (004), 48.19° (200), 54.06° (105), and 55.30° (211). Such observed major peaks were reported earlier in the literature (Esellami et al. 2018; Li and Zeng 2011). No diffractions due to impurities, rutile, or brookite were found, which is an indication of the crystallographic purity (Ratnika et al. 2010). The intensity of H1 and H2 samples is very weak, indicating low crystallinity with increasing HMTA content. Using Scherer's equation, the crystal size (calculated at 101 peak) of the synthesized anatase was 19.88 nm, 8.64 nm, 16.68 nm, and 10.25 nm for pure TiO₂, H0.5, H1, and H2, respectively. In addition, the particle sizes of TiO₂ were reduced by the addition of HMTA. In general, after the addition of HMTA, the anatase phase peak slightly shifts to the higher 2θ degree compared with pure TiO₂, suggesting the TiO₂ lattice distortion through the merging of carbon and nitrogen. The pure TiO₂ sample was fitted using FullProf software based on the Rietveld refinement method as shown in Fig. 1 B. The Rietveld refinement of the sample was consistent with XRD measurements and confirmed our findings. The crystallinity of the TiO₂ phase synthesized

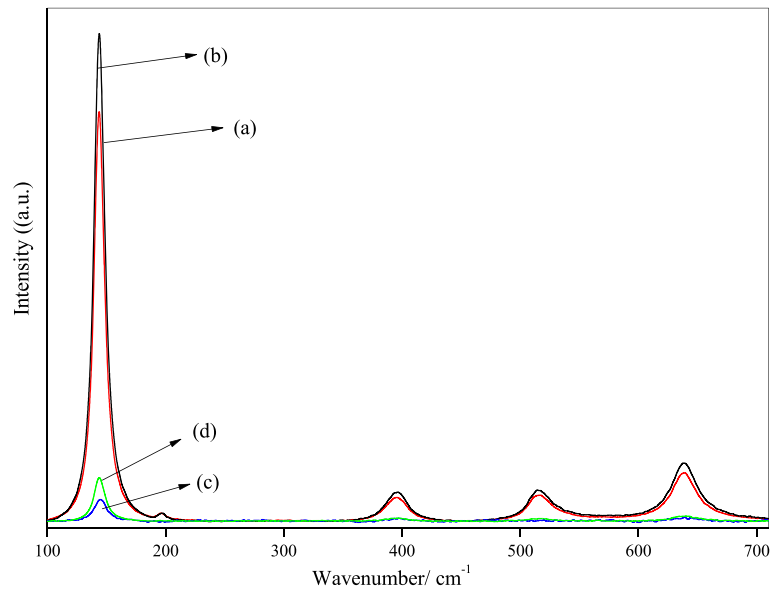
Fig. 1 **A** XRD patterns of pure TiO₂ (a) and C/N-codoped TiO₂ nanocrystals H0.5 (b), H1.0 (c), and H2.0 (d). Shifted for the sake of clarity. **B** FullProf software based on the Rietveld refinement method for pure TiO₂



by adding HMTA contents was monitored by Raman spectroscopy (Fig. 2). The findings revealed that the characteristic peaks of anatase at 144 cm^{-1} , 196.95 cm^{-1} , 394.9 cm^{-1} , 514.51 cm^{-1} , and 637.38 cm^{-1} were detected. No traces of brookite or rutile were observed. The Raman spectrum of pure TiO₂ boosted with the addition of 0.5 g HMTA; the H0.5 sample demonstrates that the obtained TiO₂ phase consisted of entirely anatase, while with increasing HMTA at 1 g (H1) and 2 g (H2), the intensity of anatase phase at 144 cm^{-1} suddenly decreased as a result of sharply decreasing crystallinity. The obtained results of Raman spectra and XRD analysis are consistent (Fig. 1).

A nitrogen adsorption–desorption hysteresis loop shapes were employed for determining the specific pore structures to explore the texture properties of the synthesized samples (Sing et al. 1985). Nitrogen adsorption isotherms of pure TiO₂, H0.5, H1, and H2 are displayed in Fig. 3. Pure TiO₂, H0.5–TiO₂, and H1–TiO₂ exhibited a typical type of IV hysteresis, suggesting narrow distributions of pore size and microporosity (Sing et al. 1985). Type IV adsorption isotherms with typical reversibility were determined for the synthesized pure TiO₂, H0.5, H1, and H2 photocatalysts. Such type is often related to porous materials or materials containing compacts or agglomerates of orderly spheres that are quite a

Fig. 2 Raman spectra of pure TiO₂ (a) and C/N-codoped TiO₂ nanocrystals H0.5 (b), H1.0 (c), and H2.0 (d)



regular array. The resulting inflection sharpness obtained from capillary condensation at relative pressures (p/p_0) between 0.42 and 0.95 is distinctive for porous structure, which is correlated to narrow slit-like pores. The synthesized pure TiO₂, H0.5, H1, and H2 photocatalysts exhibited the surface area measurements of 40.22 m² g⁻¹, 42.17 m² g⁻¹, 63.17 m² g⁻¹, and 65.57 m² g⁻¹, respectively (Table 1). The surface area measurements were promoted with the increase of HMTA contents.

Figure 4 exhibits the TEM and HRTEM images of pure TiO₂ and H0.5 samples. Pure TiO₂ without HMTA shows that the primary TiO₂ nanoparticles were clustered to obtain bigger agglomerates through the

construction TiO₂ stage itself and the size of the TiO₂ nanoparticles was estimated to be ~20 nm with spherical shape (Fig. 4a). After adding HMTA through the preparation of TiO₂ nanoparticles, the obtained TiO₂ nanoparticles have spherical morphology and uniform shape with the particle size of ~10 nm (Fig. 4c). The synthesized H0.5 nanoparticles were comparatively highly dispersed than pure TiO₂ without HMTA addition. The lower agglomeration of the TiO₂ nanoparticles in the H0.5 sample reveals that HMTA likely acts as a capping agent (Fig. 4c). HRTEM images of pure TiO₂ and H0.5 indicated anatase that is highly crystalline with some random pores as a result of TiO₂ agglomeration (Fig. 4b, d). The selected area electron diffraction (SAED) pattern of TiO₂ and H0.5 samples implying its diffraction rings precisely identifies the lattice plane of anatase phase (101) with the d spacing of ~0.354 nm (inset in Fig. 4b, d). These observations reveal the obtained samples have mesostructured along with anatase crystalline phase.

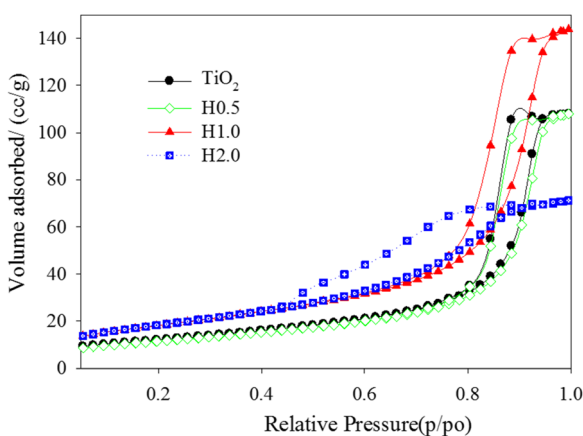


Fig. 3 N₂ sorption isotherms of pure TiO₂ and C/N-codoped TiO₂ nanocrystals H0.5, H1.0, and H2.0

XPS analysis was used for detailed investigation of H0.5 photocatalyst, which indicated high photocatalytic performance among all synthesized photocatalysts (Fig. 5). The results in Fig. 5 revealed that the sample encompasses only Ti, O, C, and traces of N. The binding energies of O 1s, Ti 2p_{3/2}, Ti 2p_{1/2}, C 1s, and N 1s are 530 eV, 459 eV, 465 eV, 285.2 eV, and 400.2 eV, respectively. XPS signals of Ti 2p were detected at binding energies at 465 eV and 459 eV for Ti 2p_{1/2} and Ti 2p_{3/2}, respectively (Fig. 5b) (Svetlozar et al. 2016; Neville et al.

Table 1 Textural properties of pure TiO₂, C/N-doped TiO₂ nanocrystals, and commercial P-25 and their photocatalytic efficiencies

| Photocatalyst | Surface area, m ² g ⁻¹ | Rate constant, min ⁻¹ (UV) | Photocatalytic efficiency, % | Rate constant, min ⁻¹ (UV-vis) | Photocatalytic efficiency, % |
|------------------|--|---------------------------------------|------------------------------|---|------------------------------|
| TiO ₂ | 40.22 | 0.0138 | 79.91 | 0.0132 | 80.17 |
| H0.5 | 42.17 | 0.0362 | 96.43 | 0.0371 | 95.70 |
| H1.0 | 63.17 | 0.0316 | 93.76 | 0.0318 | 92.66 |
| H2.0 | 65.57 | 0.0287 | 87.31 | 0.0229 | 86.90 |
| P-25 | 50.00 | 0.0048 | 54.50 | – | – |

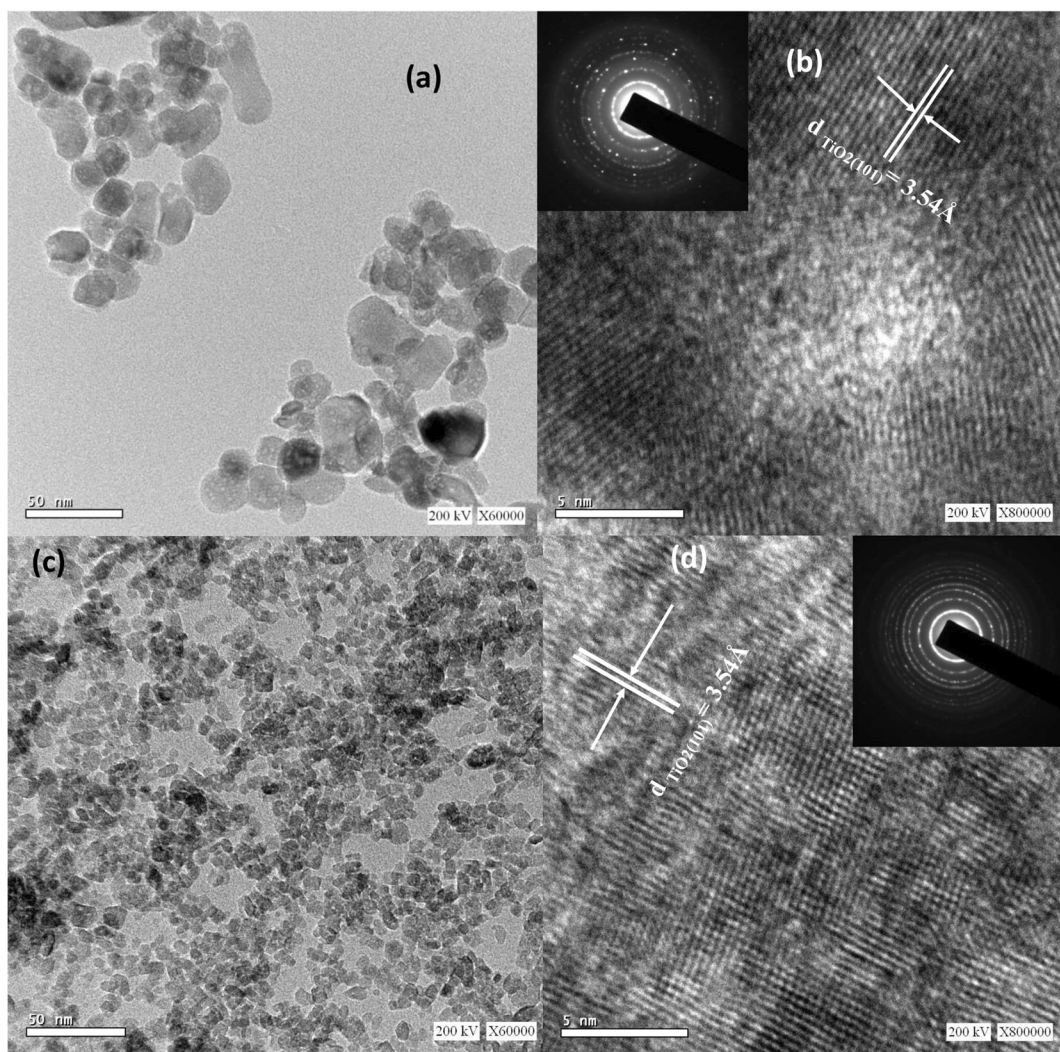


Fig. 4 TEM images of pure TiO₂ (a) and H0.5 (c) and HRTEM images of pure TiO₂ (b) and H0.5 (d). The selected area electron diffraction (SAED) pattern of TiO₂ and H0.5 samples, indicating

its diffraction rings exactly correspond to the anatase phase (101) lattice plane (fringe spacing ~0.354 nm) (inset in b and d)

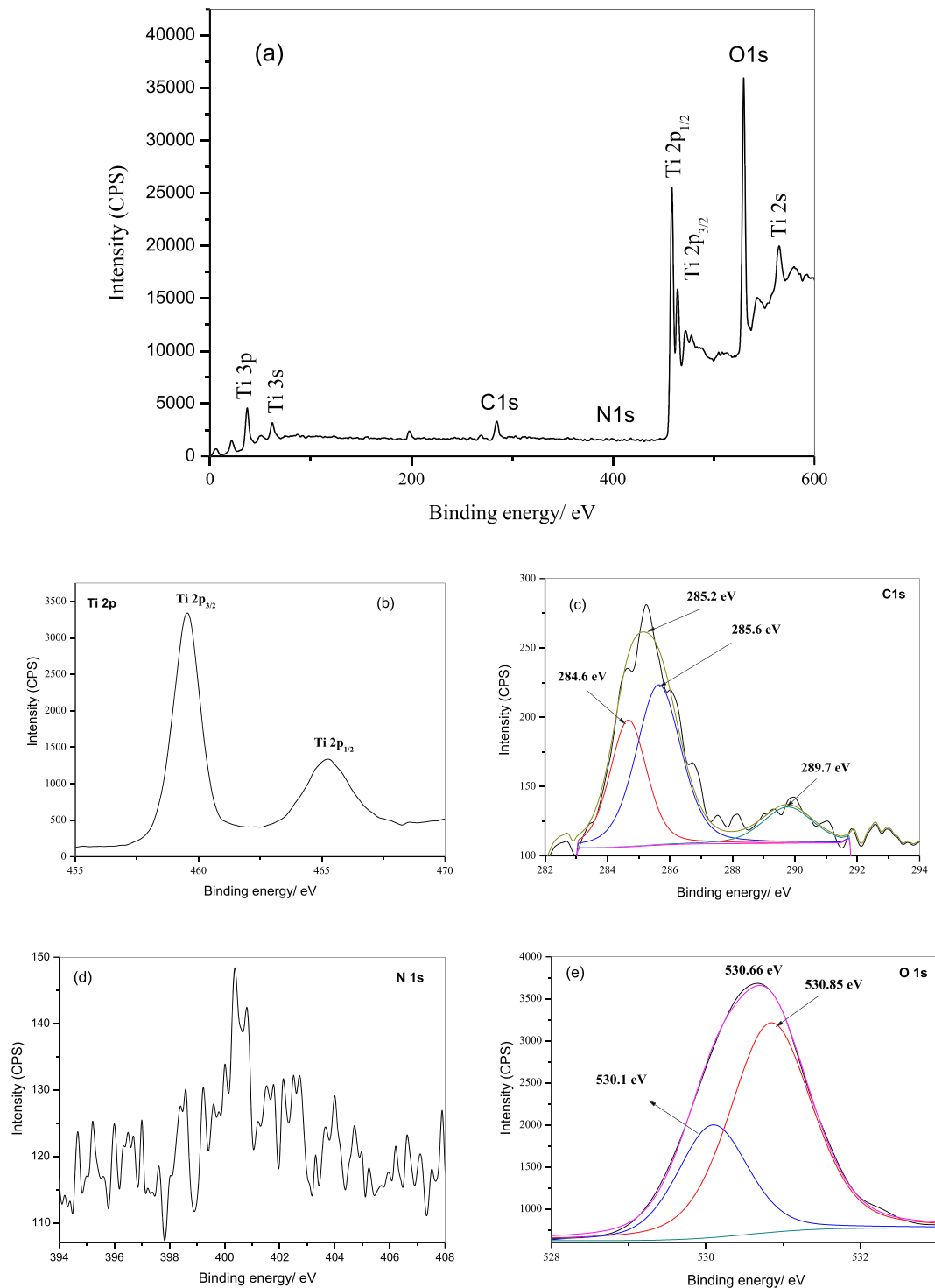


Fig. 5 XPS survey spectrum (a) and high-resolution XPS scan spectra of Ti 2p (b), C 1s (c), N 1s (d), and O 1s (e) of the H0.5 sample

2012). Detailed results also exhibited five carbon signal components at binding energies of 282.5 eV, 284.6 eV, 285.2 eV, 285.6 eV, and 289.7 eV (Fig. 5c). The assigned

peak at 284.6 eV was reported earlier as an instrumental artifact of the adventitious elemental carbon (Fig. 5c) (Eugène et al. 1995). The other peaks (285.2 eV,

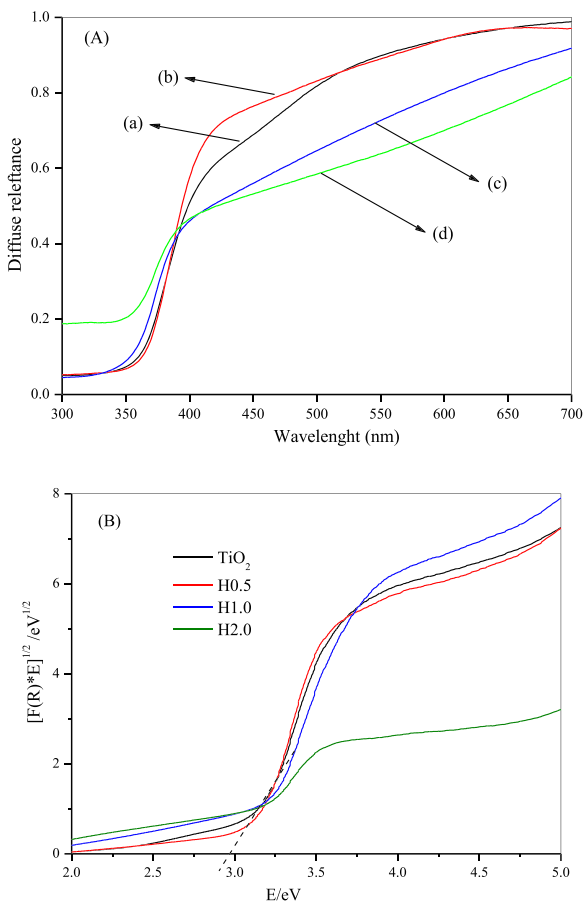


Fig. 6 **A** Diffuse reflectance spectra for the pure TiO₂ (a) and C/N-codoped TiO₂ nanocrystals H0.5 (b), H1.0 (c), and H2.0 (d). **B** Plot of transferred Kubelka–Munk versus energy of the light absorbance of pure TiO₂ and C/N-codoped TiO₂ nanocrystals H0.5, H1.0, and H2.0

285.6 eV, and 289.7 eV) were reported as the interstitial carbonate dopants and the adsorbed carbon species such as C–O and C=O onto the TiO₂ surface (Fig. 5c) (Neville et al. 2012; Yiseul et al. 2009; Sakhivel and Kisch 2003; Yuanzhi et al. 2005). The small peak at 282.5 eV was reported earlier as carbon-doped TiO₂ lattice by oxygen substitution or Ti–C, (Yin et al. 2005; In et al. 2009; Irie et al. 2006; Hsu et al. 2007). There was a weak N 1s peak detected at ~400.2 eV which can be ascribed to nitrogen species in a higher oxidation state such as N–N, N–O, and C–N bonds (Fig. 5d) (Svetlozar et al. 2016; Neville et al. 2012). This peak was normally believed to be caused by N substitution in TiO₂ or the chemisorbed nitrogen species (In et al. 2009; Irie et al. 2006; Hsu et al. 2007). The O 1s peaks are observed at 531.85 eV, 530.66 eV, and 530.10 eV as shown in Fig. 5 e. However, TiO₂ nanoparticles usually show the O 1s peak at 531.5 eV due to the

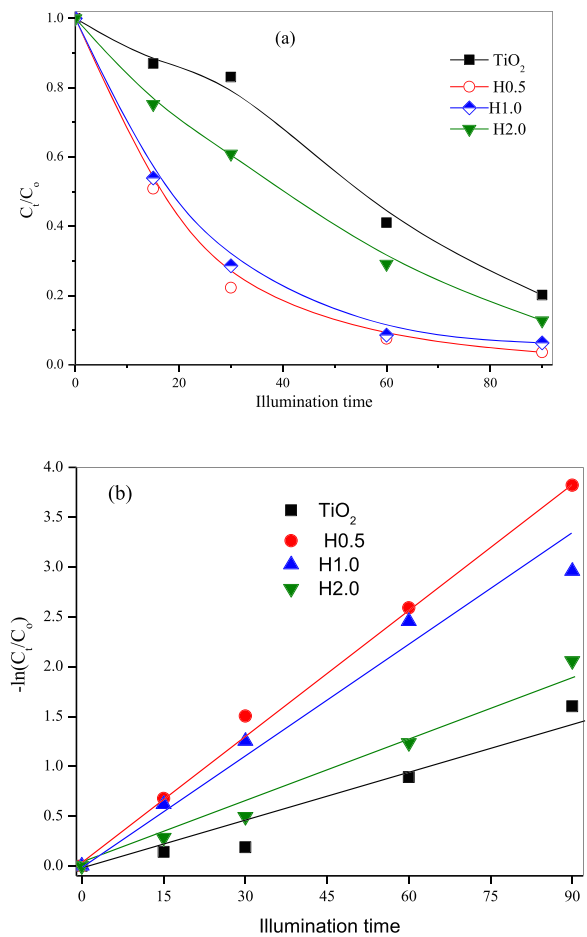


Fig. 7 Photocatalytic degradation of resorcinol over pure TiO₂ and C/N-codoped TiO₂ nanocrystals H0.5, H1.0, and H2.0 as a function of illumination time under UV light (a). $\ln(C_t/C_0)$ versus illumination time of pure TiO₂ and C/N-codoped TiO₂ nanocrystals H0.5, H1.0, and H2.0 under UV light (b)

presence of oxidized N species such as Ti–O–N being present (Beranek and Kisch 2008; Nosaka et al. 2005).

Figure 6 illustrates the UV-vis DRS of pure TiO₂, H0.5, H1, and H2 photocatalysts. DRS measurements of the synthesized samples were conducted as given in Fig. 6 A. A significant reduction in reflectance starts at about 460 nm. H0.5 and H2 samples presented the highest and lowest reflectance, respectively. The Kubelka–Munk function $F(R)$ was driven from UV-vis spectra in the diffuse reflectance mode (R) to determine the light absorption extent from scattering (Fig. 6B). The relation of the Kubelka–Munk function $(F(R)E)^{1/2}$ and the absorbed light energy (E) was used to determine the bandgap values (Fig. 6B) (Ismail et al. 2010; Lei et al. 2014; Tang et al. 1994).

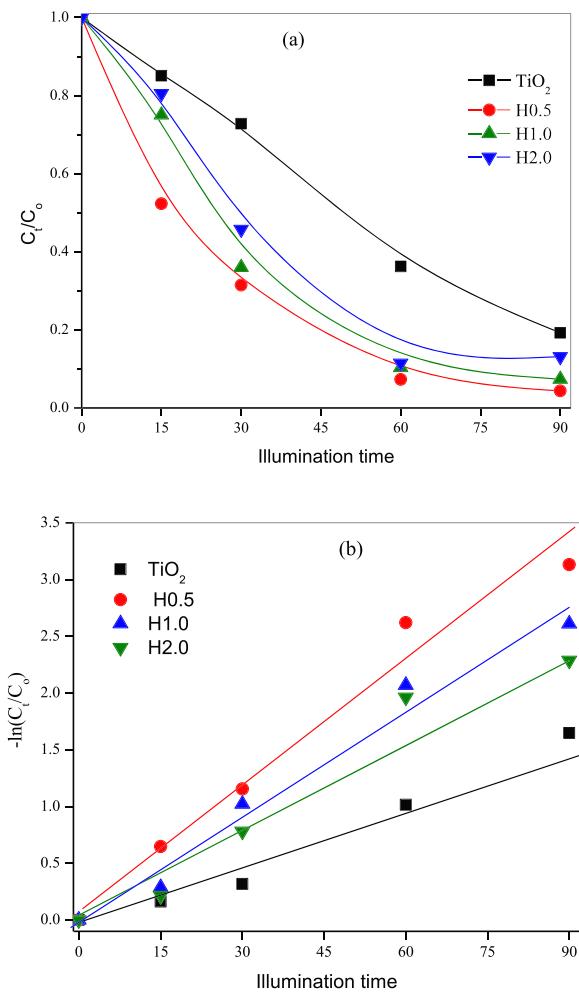


Fig. 8 Photocatalytic degradation of resorcinol over pure TiO_2 and C/N-codoped TiO_2 nanocrystals H0.5, H1.0, and H2.0 as a function of illumination time under UV-visible light (a). $\ln(C_t/C_0)$ versus illumination time of pure TiO_2 and C/N-codoped TiO_2 nanocrystals H0.5, H1.0, and H2.0 under UV-visible light (b)

$$F(R)E^{1/2} = \left(\frac{(1-R)^2}{2R} \times hv \right)^{1/2}$$

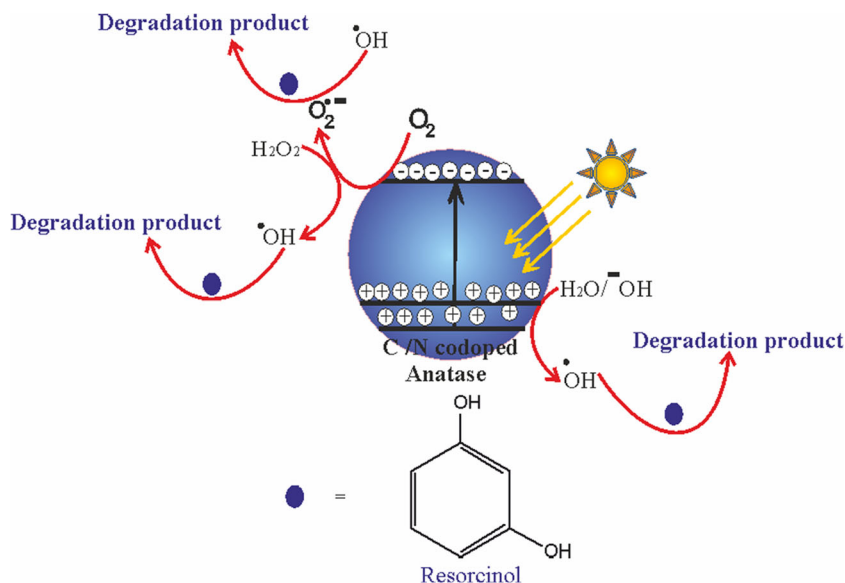
By intersecting the linear $(\alpha hv)^{1/2}$ curve part versus the photon energy axis (hv), the bandgap energies were amounted to be 3.2 eV, 2.96 ± 0.1 eV, 2.95 ± 0.1 eV, and 2.93 ± 0.1 eV for TiO_2 , H0.5, H1, and H2, respectively. E_g decreased with the increase of HMTA content from 0.5 to 2 g. Carbon and nitrogen as dopants for TiO_2 were reported earlier to reduce the bandgap energy values (Svetlozar et al. 2016; Neville et al. 2012; Eugène

et al. 1995; Yiseul et al. 2009; Sakthivel and Kisch 2003; Romualdo et al. 2004).

Photocatalytic investigations

Photocatalytic investigations of the synthesized pure TiO_2 , H0.5, H1, and H2 photocatalysts were conducted for photodegradation of resorcinol in aerated aqueous solution under UV and UV-vis light illuminations (Figs. 7 and 8) under the following conditions: pH value ~ 7 , resorcinol concentration of 20 ppm, and 1 g/L photocatalyst dosage. As previously reported by the researchers, resorcinol adsorption by C/N-codoped TiO_2 nanocrystals was dependent on complicated parameters such as ambient pH values, adsorbent doses, and surface charge of nanomaterials; generally, the adsorptive capacity of C/N-codoped TiO_2 nanocrystals was nearly equilibrated within 30 min (Xiao et al. 2008). In the photocatalytic measurements before illumination, the mixture was stirred which was employed at room temperature in the dark for 30 min to obtain an equilibrium of adsorption/desorption between the photocatalyst surfaces and resorcinol. The findings showed that the adsorption of resorcinol over the synthesized photocatalysts was less than 5%. On the other hand, photolysis of resorcinol without catalysts was insignificant within 2 h under UV illumination. At UV illumination, the photocatalytic efficiencies of the pure TiO_2 , H0.5, H1, and H2 photocatalysts were amounted to be 79.91%, 96.43%, 93.76%, and 87.31%, respectively, as displayed in Fig. 7 a; however, the photocatalytic efficiency of commercial TiO_2 was 54.50%. The H0.5 photocatalyst was achieved up to 96% within 90 min, while the photocatalytic efficiency based on the commercial P-25 was 54% (Table 1). In case of UV-vis light, the photocatalytic efficiency of pure TiO_2 , H0.5, H1, and H2 photocatalysts was amounted to be 80.17%, 95.70%, 92.66%, and 86.90%, respectively, as shown in Fig. 8 a. For resorcinol photodegradation in aerated aqueous solution under either UV or UV-vis illumination, C/N-codoped TiO_2 nanocrystals synthesized at 0.5 g HMTA exhibited the highest photocatalytic efficiency among all synthesized samples. At 0.5 g amount of HMTA addition, the H0.5 photocatalyst showed the outstanding photocatalytic efficiency of $\sim 96.43\%$, which was 1.2 and 2 times greater than that of commercial P-25 and pure TiO_2 . The photocatalytic efficiency of C/N-codoped TiO_2 was considerably enhanced due to the increase of photogenerated

Scheme 1 Mechanism diagram of photocatalytic degradation of resorcinol over carbon and nitrogen-doped TiO₂ under UV illumination



charge separation rate, smaller crystal size, narrower bandgap energy and stronger light harvesting in broad visible region, and synergism effect.

To examine the photodegradation rate qualitatively of resorcinol throughout UV and UV-vis illumination, the photodegradation of pollutants can be explained by a pseudo-first-order reaction employing the Langmuir–Hinshelwood model: $Kt = \ln C/C_0$ (Khedr et al. 2019; El-Sheikh et al. 2017; Nosaka et al. 2005), where C_0 , C , and k are the initial resorcinol concentration, the resorcinol concentration in solution at a specific time, and the apparent first-order rate constant, respectively. The linear relationship of the logarithm of the ratio between the initial resorcinol concentration and its concentration at interval times ($\ln C/C_0$) against the illumination time is depicted in Figs. 7 b and 8 b. The apparent rate constants for resorcinol photodegradation are summarized in Table 1. The findings revealed that the photocatalytic reaction of the pure TiO₂, H0.5, H1, and H2 photocatalysts followed a pseudo-first-order reaction (Fig. 7b) (Zhang et al. 2018; Cheng et al. 2017); the rate constants (k) of resorcinol degradation over pure TiO₂, H0.5, H1, and H2 photocatalysts were estimated to be 0.0138 min⁻¹, 0.0362 min⁻¹, 0.0316 min⁻¹, and 0.0287 min⁻¹, respectively, and the rate constant of the photocatalytic efficiency of commercially available photocatalyst P-25 was 0.0048 min⁻¹. The H0.5 rate constant was 3 and 7.5 times greater than that of pure TiO₂ and commercial P-25, respectively. In case of UV-vis illumination, the rate constants (k) of resorcinol

degradation over pure TiO₂, H0.5, H1, and H2 photocatalysts were amounted to be 0.0132 min⁻¹, 0.0371 min⁻¹, 0.0318 min⁻¹, and 0.0229 min⁻¹, respectively (Table 1, Fig. 8b). The reaction rate of the H0.5 sample was 3 times higher than that of pure TiO₂ under UV-vis illumination.

When the UV-vis light attacks the C/N-codoped TiO₂ surface, the produced photogenerated electrons were transferred by two various avenues. In the first expected avenue, the intra-bandgap states approaching the valence band levels can be created by doping carbon and

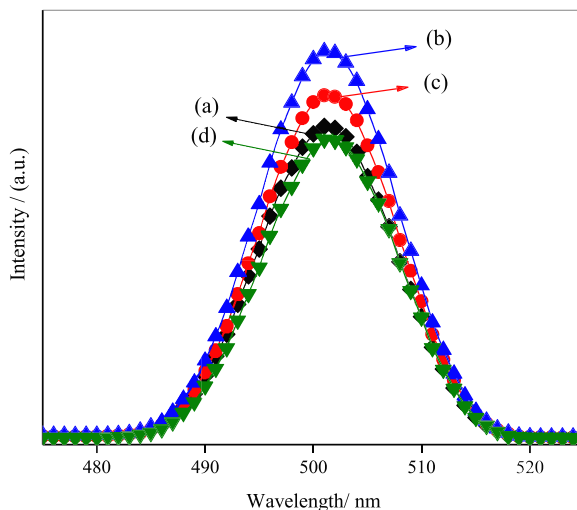


Fig. 9 Photoluminescence (PL) of pure TiO₂ (a) and C and N-codoped TiO₂ nanocrystals H0.5 (b), H1.0 (c), and H2.0 (d) obtained at an excitation 320 nm wavelength

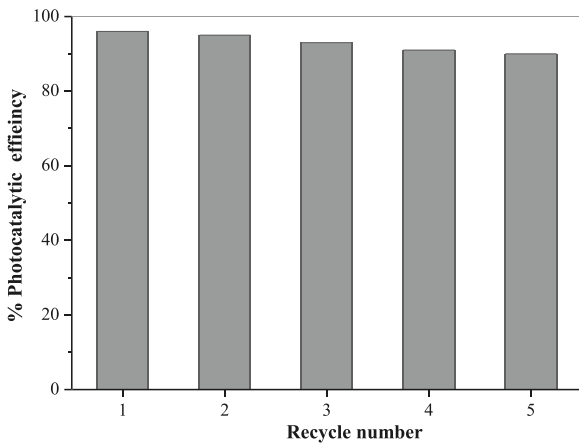
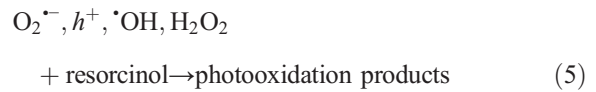


Fig. 10 Reusability up to 5 times of photocatalytic degradation of resorcinol over H0.5

nitrogen to the TiO₂ (Scheme 1), and the location of flat band potential level rises the TiO₂ conduction band (Saïen and Mesgari 2016). Therefore, when the UV-vis light illuminates the C/N-codoped TiO₂ surface, the electrons are moved smoothly from the intra-bandgap to flat band (Saïen and Mesgari 2016; Del Ángel-Sanchez et al. 2013). In the second expected avenue, when the C/N-codoped TiO₂ surface illuminated by UV-vis light, photo-induced electrons are created (Eq. (1)). Then, the photogenerated electrons move to flat band of N-TiO₂ or the conduction band. The adsorbed molecular O₂ onto the photocatalyst surface can be reduced by the reactive electrons produced on the flat band of C/N-TiO₂ and conduction band to O₂^{•-} radical, which create HO[•] radical throughout a chain of reactions, indicating the oxidation of resorcinol in the ultimate stage (Shulian et al. 2011; Shao et al. 2015; Nawawi and Nawi 2014; Ismail et al. 2009). Meanwhile, the active radical species [•]OH and O₂^{•-} in addition to H₂O₂ (Ismail et al. 2010) (Eqs. (2)–(4)) can degrade resorcinol to its radical cation by the H₂O oxidation (Eq. (5)). Carbon and nitrogen act as the synergistic effect in which carbon harvested the light, and the produced photogenerated electrons are moved to the conduction band of nitrogen/TiO₂ photocatalyst to expedite the photoreaction and complete resorcinol photodegradation.



To confirm and explore the mechanism complete photodegradation of resorcinol over the H0.5 photocatalyst, PL spectra for pure TiO₂, H0.5, H1, and H2 samples were conducted and are displayed in Fig. 9. The findings exhibited higher PL intensity of H0.5 and H1 samples than pure TiO₂; however, PL intensity of the H2 sample is smaller than pure TiO₂. The highest amount of nitrogen and the low content of carbon-doped TiO₂ have the highest PL intensity. Therefore, the H0.5 photocatalyst possessed the best photocatalytic efficiency among all synthesized photocatalysts as aforementioned above. The excitonic PL was boosted by the decrease of dopant carbon content as shown in the H0.5 sample. However, the excitonic PL for the H2 sample was minimal than that for the pure TiO₂ samples. This is explained by the presence of high carbon content onto the TiO₂ surface of the H2 sample than either H0.5 or H1 sample. Lower carbon content at the H0.5 sample can expedite the separation of charge carriers since carbon can play as an electron scavenger (Janus et al. 2006). Therefore, two main phenomena took place concurrently in the C/N-TiO₂: (i) The excitonic PL intensity increases by nitrogen doping of pure TiO₂ due to boosting defect state and (ii) the presence of carbon content onto nitrogen/TiO₂ prohibits recombination of electron hole (Wu et al. 2008). On both cases, the overall effectiveness is to substantially prevent the recombination of charge carriers within the C/N-codoped TiO₂ photocatalyst.

To examine the reducibility and stability of the H0.5 sample, it was used with repeating for resorcinol degradation (Fig. 10). The resorcinol solution and H0.5 sample were mixed and aerated, employing a pump to provide oxygen throughout photocatalytic reactions. At the end of each

experiment, the H0.5 photocatalyst was separated and washed three times with ethanol and water and finally was dried. The photocatalytic degradation of resorcinol over the H0.5 sample was employed again (5 times). The findings revealed a 96% photocatalytic degradation slightly minimized to 91% (Fig. 10), confirming that H0.5 could be reused five times without considerable loss to the photocatalytic activity. C/N–TiO₂ nanocrystal is an effective and stable photocatalyst, characteristic for the photodegradation of toxic organic contaminants in industrial wastewater in the presence of UV and visible light illumination.

Conclusions

Carbon species and nitrogen-codoped anatase TiO₂ nanocrystals are synthesized by the solvothermal process in the existence of HMTA. The photocatalytic performance of the C/N–TiO₂ nanocrystals was examined for resorcinol degradation under UV-vis illumination. The H0.5 photocatalyst exhibited the outstanding photocatalytic performance, which is 1.2 and 2 times greater than that of commercial P-25 and pure TiO₂. In addition, the rate constant of the H0.5 sample was enhanced 7.5 and 3 times than that of commercial P-25 and pure TiO₂, respectively. The photocatalytic efficiency of C/N-codoped TiO₂ was considerably improved due to the increase of photogenerated charge separation rate, smaller crystal size, narrower bandgap energy, and stronger light harvesting in the broad visible region. Therefore, the C/N-codoped TiO₂ nanocrystal exhibited high capacities to become an efficient photocatalyst with stability and high photocatalytic activity under UV-vis illumination.

Acknowledgments Kuwait Institute for Scientific Research (KISR) is gratefully acknowledged for the instrumental facilities.

Funding information The study received financial support from the Kuwait Foundation for the Advancement of Sciences (KFAS) related to the Project EA071C under the contract number PR17-12SC-01.

Compliance with ethical standards

Conflict of interest The authors declare that they have no conflict of interest.

References

- Ahmad ZU, Lian Q, Zappi ME, Buchireddy PR, Gang DD (2019) Adsorptive removal of resorcinol onto surface modified ordered mesoporous carbon: kinetics and equilibrium study. *Environ Prog Sustain Energy* 38:S386–S397
- Al-Hajji LA, Ismail AA, Al-Hazza A, Ahmed SA, Alsaïdi M, Almutawa F, Bumajdad A (2020) Impact of calcination of hydrothermally synthesized TiO₂ nanowires on their photocatalytic efficiency. *J Mol Struct* 1200:127153
- Atitar MF, Ismail AA, Al-Sayari SA, Bahneman D, Afanasev D, Emeline AV (2015) Mesoporous TiO₂ nanocrystals as efficient photocatalysts: impact of calcination temperatures and phase transformations on photocatalytic performances. *Chem Eng J* 264:417–424
- Atitar MF, Ismail AA, Dillert R, Bahnemann DW (2019) Photodegradation of herbicide imazapyr and phenol over mesoporous bicrystalline phases TiO₂: a kinetic study. *Catalysts* 9:640
- Beranek R, Kisch H (2008) Tuning the optical and photoelectrochemical properties of surface-modified TiO₂. *Photochem Photobiol Sci* 7:40–48
- Bilgili MS (2006) Adsorption of 4-chlorophenol from aqueous solutions by xad-4 resin: isotherm, kinetic, and thermodynamic analysis. *J Hazard Mater* 137:157–164
- Busca G, Berardinelli S, Resini C, Arrighi L (2008) Technologies for the removal of phenol from fluid streams: a short review of recent developments. *J Hazard Mater* 160:265–288
- Candelaria SL, Garcia BB, Liu D, Cao G (2012) Nitrogen modification of highly porous carbon for improved supercapacitor performance. *J Mater Chem* 22:9884–9889
- Cheng P, Deng C, Gu M, Dai X (2008) Effect of urea on the photoactivity of titania powder prepared by sol-gel method. *Mater Chem Phys* 107:77–81
- Cheng L, Qiu S, Chen J, Shao J, Cao S (2017) A practical pathway for the preparation of Fe₂O₃ decorated TiO₂ photocatalyst with enhanced visible-light photoactivity. *Mater Chem Phys* 190:53–61
- Dąbrowski A, Podkościelny P, Hubicki Z, Barczak M (2005) Adsorption of phenolic compounds by activated carbon—a critical review. *Chemosphere* 58:1049–1070
- Del Ángel-Sánchez K, Vázquez-Cuchillo O, Aguilar-Elguezabal A, Cruz-López A, Herrera-Gómez A (2013) Photocatalytic degradation of 2,4-dichlorophenoxyacetic acid under visible light: effect of synthesis route. *Mater Chem Phys* 139:423–430
- Dreyfors JM, Jones SB, Sayed Y (1989) Hexamethylenetetramine: a review. *Am Ind Hyg Assoc J* 50:579–585
- Elsellami L, Dappozze F, Fessi N, Houas A, Guillard C (2018) Highly photocatalytic activity of nanocrystalline TiO₂ (anatase, rutile) powders prepared from TiCl₄ by sol-gel method in aqueous solutions. *Process Saf Environ Prot* 113:109–121
- El-Sheikh SM, Zhang G, El-Hosainy HM, Ismail AA, O’Shea K, Falaras P, Kontos AG, Dionysiou DD (2014) High performance, sulfur, nitrogen and carbon doped mesoporous anatase-brookite TiO₂ photocatalyst for the removal of microcystin-LR under visible light irradiation. *J Hazard Mater* 280:723–733

- El-Sheikh SM, Khedr TM, Hakki A, Ismail AA, Badawy WA, Bahnemann DW (2017) Visible light activated carbon and nitrogen co-doped mesoporous TiO₂ as efficient photocatalyst for degradation of ibuprofen. *Sep Purif Technol* 173:258–268
- Eugène P, Lacroix R, Donnet J-B, Nansé G, Fioux P (1995) XPS study of the halogenation of carbon black—part 2. Chlorination. *Carbon* 33:63–72
- Fujishima A, Zhang X (2006) Titanium dioxide photocatalysis: present situation and future approaches. *C R Chim* 9:750–760
- Hsu S-W, Yang T-S, Chen T-K, Wong M-S (2007) Ion-assisted electron-beam evaporation of carbon-doped titanium oxide films as visible-light photocatalyst. *Thin Solid Films* 515: 3521–3526
- In S-I, Kean AH, Orlov A, Tikhov MS, Lambert RM (2009) A versatile new method for synthesis and deposition of doped, visible light-activated TiO₂ thin films. *Energy Environ Sci* 2: 1277–1279
- Irie H, Washizuka S, Hashimoto K (2006) Hydrophilicity on carbon-doped TiO₂ thin films under visible light. *Thin Solid Films* 510:21–25
- Ismail AA, Bahnemann DW, Bannat I, Wark M (2009) Gold nanoparticles on mesoporous interparticle networks of titanium dioxide nanocrystals for enhanced photonic efficiencies. *J Phys Chem C* 113:7429–7435
- Ismail AA, Bahnemann DW, Robben L, Yarovy V, Wark M (2010) Palladium doped porous titania photocatalysts: impact of mesoporous order and crystallinity. *Chem Mater* 22: 108–116
- Janus M, Inagaki M, Tryba B, Toyoda M, Morawski AW (2006) Carbon-modified TiO₂ photocatalyst by ethanol carbonisation. *Appl Catal B: Environ* 63:272–276
- Khedr TM, El-Sheikh SM, Ismail AA, Kowalska E, Bahnemann DW (2019) Photodegradation of microcystin-LR using visible light-activated C/N-co-modified mesoporous TiO₂ photocatalyst. *Materials* 12:1027
- Ku Y, Lee KC (2000) Removal of phenols from aqueous solution by XAD-4 resin. *J Hazard Mater* 80:59–68
- Kumar A, Kumar S, Kumar S (2003) Adsorption of resorcinol and catechol on granular activated carbon: equilibrium and kinetics. *Carbon* 41:3015–3025
- Lei XF, Xue XX, Yang H (2014) Preparation and characterization of Ag-doped TiO₂ nanomaterials and their photocatalytic reduction of Cr(VI) under visible light. *Appl Surf Sci* 321: 396–403
- Li W, Zeng T (2011) Preparation of TiO₂ anatase nanocrystals by TiCl₄ hydrolysis with additive H₂SO₄. *PLoS One* 6:21082
- Liu G, Zhao Y, Sun C, Li F, Lu GQ, Cheng HM (2008) Synergistic effects of B/N doping on the visible-light photocatalytic activity of mesoporous TiO₂. *Angew Chem Int Ed* 47: 4516–4520
- Liu J, Qin W, Zuo S, Yu Y, Hao Z (2009) Solvothermal-induced phase transition and visible photocatalytic activity of nitrogen-doped titania. *J Hazard Mater* 163:273–278
- Mohanty K, Jha M, Meikap BC, Biswas MN (2005) Preparation and characterization of activated carbons from terminalia arjuna nut with zinc chloride activation for the removal of phenol from wastewater. *Ind Eng Chem Res* 44:4128–4138
- Naik B, Parida KM, Gopinath CS (2010) Nanocrystalline TiO₂ and direct solar-light-driven photocatalytic activity. *J Phys Chem C* 114:19473–19482
- Nawawi WI, Nawi MA (2014) Carbon coated nitrogen doped P25 for the photocatalytic removal of organic pollutants under solar and low energy visible light irradiations. *J Mol Catal A Chem* 383–384:83–93
- Neville EM, Mattle MJ, Loughrey D, Rajesh B, Rahman M, MacElroy JMD, Sullivan JA, Thampi KR (2012) Carbon-doped TiO₂ and carbon, tungsten-codoped TiO₂ through sol-gel processes in the presence of melamine borate: reflections through photocatalysis. *J Phys Chem C* 116:16511–16521
- Nosaka Y, Matsushita M, Nishino J, Nosaka AY (2005) Nitrogen-doped titanium dioxide photocatalysts for visible response prepared by using organic compounds. *Sci Technol Adv Mater* 6:143
- Ohko Y, Ando I, Niwa C, Tatsuma T, Yamamura T, Nakashima T, Kubota Y, Fujishima A (2001) Degradation of bisphenol A in water by TiO₂ photocatalyst. *Environ Sci Technol* 35: 2365–2368
- Ratnika V, Bhaduria S, Gaur MS (2010) Biogenic synthesis of silver nanocubes and nanorods using sundried Stevia rebaudiana leaves. *Adv Mat Lett* 1:232–237
- Rodriguez-Carvajal J (1993) Recent advances in magnetic structure determination by neutron powder diffraction. *Phys B* 192:55–69
- Romualdo TG, Lindgren T, Lu J, Granqvist C-G, Lindquist S-E (2004) Photoelectrochemical study of nitrogen-doped titanium dioxide for water oxidation. *J Phys Chem B* 108:5995–6003
- Saien J, Mesgari Z (2016) Highly efficient visible-light photocatalyst of nitrogen-doped TiO₂ nanoparticles sensitized by hematoporphyrin. *J Molecular Catalysis A: Chemical* 414:108–115
- Sakthivel S, Kisch H (2003) Daylight photocatalysis by carbon-modified titanium dioxide. *Angew Chem Int Ed* 42:4908–4911
- Shao Y, Cao C, Chen S, He M, Fang J, Chen J, Li X, Li D (2015) Investigation of nitrogen doped and carbon species decorated TiO₂ with enhanced visible light photocatalytic activity by using chitosan. *Appl Catal B: Environ* 179:344–351
- Shulian W, Yanfen F, Yong Y, Junzi L, Ping DA, Rong ZX, Ping HY (2011) Catalysis of organic pollutant photodegradation by metal phthalocyanines immobilized on TiO₂@SiO₂. *Chin Sci Bull* 56:969–976
- Sing KSW, Everett DH, Haul RAW et al (1985) Reporting physisorption data for gas/solid systems with special reference to the determination of surface area and porosity. *Pure Appl Chem* 57:603–619
- Svetlozar I, Barylyak A, Besaha K, Bund A, Bobitski Y, Wojnarowska-Nowak R, Yaremchuk I, Kus-Liškiewicz M (2016) Synthesis, characterization, and photocatalytic properties of sulfur and carbon-codoped TiO₂ nanoparticles. *Nanoscale Res Lett* 11:140
- Tang H, Prasad K, Sanilines R, Schmid PE, Levy F (1994) Electrical and optical properties of TiO₂ anatase thin films. *J Appl Phys* 75:2042–2047
- Wu Z, Dong F, Zhao W, Guo S (2008) Visible light induced electron transfer process over nitrogen doped TiO₂ nanocrystals prepared by oxidation of titanium nitride. *J Hazard Mater* 157:57–63

- Xiao Q, Zhang J, Xiao C, Si Z, Tan X (2008) Solar photocatalytic degradation of methylene blue in carbon-doped TiO₂ nanoparticles suspension. *Sol Energy* 82:706–713
- Xu H, Zhang L (2010) Selective nonaqueous synthesis of C-Cl-codoped TiO₂ with visible-light photocatalytic activity. *J Phys Chem C* 114:11534–11541
- Yin S, Yamaki H, Komatsu M, Zhang Q, Wang J, Tang Q, Saito F, Sato T (2003) Preparation of nitrogen-doped titania with high visible light induced photocatalytic activity by mechanochemical reaction of titania and hexamethylenetetramine. *J Mater Chem* 13:2996–3001
- Yin S, Aita Y, Komatsu M, Wang J, Tang Q, Sato T (2005) Synthesis of excellent visible-light responsive TiO_{2-x}N_y photocatalyst by a homogeneous precipitation-solvothermal process. *J Mater Chem* 15:674–682
- Yiseul P, Kim W, Park H, Tachikawa T, Majima T, Choi W (2009) Carbon-doped TiO₂ photocatalyst synthesized without using an external carbon precursor and the visible light activity. *Appl Catal B Environ* 91:355–361
- Yuanzhi L, Hwang D-S, Lee NH, Kim S-J (2005) Synthesis and characterization of carbon-doped titania as an artificial solar light sensitive photocatalyst. *Chem Phys Lett* 404:25–29
- Zhang Y, Chen J, Tang H, Xiao Y, Qiu S, Li S, Cao S (2018) Hierarchically-structured SiO₂-Ag@TiO₂ hollow spheres with excellent photocatalytic activity and recyclability. *J Hazard Mater* 354:17–26

Publisher's note Springer Nature remains neutral with regard to jurisdictional claims in published maps and institutional affiliations.